Tunable Thin-Film Crystalline Structures and Field-Effect Mobility of Oligofluorene–Thiophene Derivatives

Tae Joo Shin,*[,†] Hoichang Yang,[‡] Mang-mang Ling,[§] Jason Locklin,[§] Lin Yang,[||] Byeongdu Lee,[⊥] Mark E. Roberts,[§] Abhijit Basu Mallik,[§] and Zhenan Bao*[,§]

Pohang Accelerator Laboratory, Pohang, Kyungbuk 790-784, Korea, and Rensselaer Nanotechnology Center, Rensselaer Polytechnic Institute, Troy, New York 12180, Department of Chemical Engineering, Stanford University, Stanford, California 94305, National Synchrotron Light Source, Brookhaven National Laboratory, Upton, New York 11973, Advanced Photon Source, Argonne National Laboratory, Argonne, Illinois 60439

Received April 18, 2007. Revised Manuscript Received August 27, 2007

Air-stable *p*-type semiconducting oligofluorene–thiophene derivatives were vacuum-deposited on octadecyltriethoxysilane-treated SiO_2/Si substrates. Effects of end-substituents and substrate deposition temperature (T_D) on molecular orientation, crystalline morphologies, and structures in these thin films were investigated by two-dimensional grazing incidence X-ray diffraction and atomic force microscopy, and those results were correlated with charge mobility in top-contacted devices. Crystalline morphologies of the first monolayer thin film in direct contact with the dielectric surface, influenced by T_Ds (25, 90, and 140 °C) and end-substituted groups (hydrogen, hexyl, and dodecyl), could be categorized as dendrite, compact disk, and single-crystal-like layered grains. The results of grazing incidence X-ray diffraction strongly support that molecular orientation in the films can be finely tuned through controlling substrate, T_D, and molecular architecture, resulting in high air stability and field-effect mobility in a top-contacted electrode of organic thin film transistors.

Introduction

Organic thin film transistors (OTFTs) have received considerable attention for various applications, such as flexible flat panel displays, electronic paper, organic light-emitting diodes, smart cards, smart inventory tags, intelligent sensor arrays, etc.[1–4] The performance of OTFTs has improved dramatically over the past few years, and many OTFTs based on new materials have shown electrical characteristics comparable to hydrogenated amorphous silicon-based TFTs. Many efforts are still in progress to further understand how the molecular structures of organic thin films correlate to the electrical properties of the corresponding OTFTs. X-ray diffraction and AFM techniques have generally been used to study crystalline structures and surface morphologies. Although AFM has been able to investigate morphologies from submonolayer (sub-ML) to multilayers, most X-ray diffraction studies have been confined to relatively thick films. It has been suggested that the charge-carrier transport in OTFT devices primarily occurs in the first few molecular layers in proximity to the gate dielectric layer.[5–8] Therefore, structural and morphological studies should be performed on ultrathin layers (<5 nm) to provide insight to the origin of the 'structure–property relationship, and further for the optimization of processing conditions of devices and the modification of semiconducting materials.

Recently, Fritz et al. reported a polymorphic structure of a crystal in pentacene thin films, so-called "thin film phase", which is much different from a triclinic "bulk phase".[9,10] In the thin film phase, a molecular axis is oriented nearly normal to the substrate (edge-on structure) and π–π stacking planes are parallel to the charge-transport direction. For a thin film phase of pentacene crystal, an orthorhombic polymorph has been also proposed for films with thickness below 100 nm.[11] The interaction between the first seeding molecules (i.e., the initial nucleus) and the dielectric layer strongly affects the formation of the metastable thin film phase, where predominant (*001*) crystal planes have thermodynamically the lowest surface energy. A correlation between the crystalline structures in sub-ML pentacene films and the field-effect mobility has been studied using two-dimensional grazing incidence

* Corresponding author. E-mail: stj@postech.ac.kr (T.J.S.); zbao@stanford.edu (Z.B.).
† Pohang Accelerator Laboratory.
‡ Rensselaer Polytechnic Institute.
§ Stanford University.
|| Brookhaven National Laboratory.
⊥ Argonne National Laboratory.

(1) Ling, M. M.; Bao, Z. N. *Chem. Mater.* **2004**, *16*, 4824–4840.
(2) Dimitrakopoulos, C. D.; Malenfant, P. R. L. *Adv. Mater.* **2002**, *14*, 99–117.
(3) Newman, C. R.; Frisbie, C. D.; da Silva Filho, D. A.; Bredas, J. L.; Ewbank, P. C.; Mann, K. R. *Chem. Mater.* **2004**, *16*, 4436–4451.
(4) Klauk, H.; Schmid, G.; Radlik, W.; Weber, W.; Zhou, L. S.; Sheraw, C. D.; Nichols, J. A.; Jackson, T. N. *Solid-State Electron.* **2003**, *47*, 297–301.
(5) Katz, H. E.; Bao, Z. *J Phys. Chem. B* **2000**, *104*, 671–678.
(6) Horowitz, G.; Hajlaoui, M. E. *Adv. Mater.* **2000**, *12*, 1046–1050.
(7) Kulkarni, A. P.; Tonzola, C. J.; Babel, A.; Jenekhe, S. A. *Chem. Mater.* **2004**, *16*, 4556–4573.
(8) Alam, M. A.; Dodabalapur, A.; Pinto, M. R. *IEEE Trans. Electron Devices* **1997**, *44*, 1332–1337.
(9) Fritz, S. E.; Martin, S. M.; Frisbie, C. D.; Ward, M. D.; Toney, M. F. *J. Am. Chem. Soc.* **2004**, *126*, 4084–4085.
(10) Ruiz, R.; Mayer, A. C.; Malliaras, G. G.; Nickel, B.; Scoles, G.; Kazimirov, A.; Kim, H.; Headrick, R. L.; Islam, Z. *Appl. Phys. Lett.* **2004**, *85*, 4926–4928.
(11) Drummy, L. F.; Martin, D. C. *Adv. Mater.* **2005**, *17*, 903–907.

10.1021/cm0710599 CCC: $37.00
Published on Web 10/30/2007

X-ray diffraction (2D GIXD) and atomic force microscopy (AFM) for OTFT applications.[12] In that study, we have shown that the field-effect mobility of the OTFT comprised of single-crystal-like faceted islands as the first monolayer results in higher mobility than that of dendritic islands type, suggesting the importance of grain shape and perfectness for effective intra- and intercontact between grains.

In addition to high charge mobility, air stability is an important requirement for the design of organic semiconductor materials for commercial OTFT applications. It has been reported that humidity and light seriously degrade the electrical performance of pentacene thin films.[13–17] On the basis of their ambient stability, oligofluorene–thiophene derivatives are promising for OTFT applications. For example, 5,5′-bis(7-hexyl-9*H*-fluoren-2-yl)-2,2′-bithiophene (DHFTTF) thin films in OTFTs have shown high charge mobility ($\sim$0.1 cm^2 V^{-1} s^{-1}) and on/off ratio ($\sim 1 \times 10^5$) for devices stored in air with exposure to ambient light for several months.[18–20]

In the present study, molecular orientation and crystalline structures in thin films of three different oligofluorene–thiophene derivatives have been investigated using a 2D GIXD technique[21] and their morphologies by AFM. Monolayers comprised of 2D crystals[22] do not provide a sufficient X-ray diffraction signal for a direct determination of the atomic positions as in 3D crystals. Nevertheless, using fixed atomic coordinate models for the self-assembled molecules, it is possible to extract valuable information, such as the unit-cell parameters, crystal-packing arrangement, and molecular tilt direction and its angle in 2D crystals. Our studies are specifically focused on tunable crystalline structures and morphologies of thin films caused by alkyl end-substitutions (hydrogen, hexyl, and dodecyl) and substrate deposition temperature (T_D = 25, 90, and 140 °C). Furthermore, those characteristics are correlated with the charge mobility in top-contacted OTFTs.

2D GIXD Analysis

The intensity, $I(q_{xy}, q_z)$, in 2D GIXD is simultaneously acquired as a function of in-plane (q_{xy}) and out-of-plane (q_z) components of the scattering vector. Becuase in-plane orientations of crystalline domains made by vacuum deposition are random, the in-plane component in 2D GIXD patterns is the sum of all those different orientations. Therefore, q_{xy} is represented as a combination of q_x and q_y, $q_{xy} = \sqrt{q_x^2+q_y^2}$, without a distinction between those two components, whereas its out-of-plane component, q_z, is measured directly. The diffraction condition for 2D crystals in the *xy* plane is that a q_{xy} vector ($q_{xy} \approx 4\pi \sin(\theta/\lambda)$, where 2θ is the horizontal angle between the incident and the diffracted beam) should coincide with a reciprocal lattice vector G_{hk} ($G_{hk} = 2\pi(ha^* + kb^*)$, where a^* and b^* are the reciprocal unit vectors and h and k are the integers). On the contrary, there is no selection rule or restriction on the scattering vector component along the surface normal, q_z ($q_z \approx 2\pi \sin(\alpha_f/\lambda)$, where α_f is the angle between the diffracted beam and the flat substrate).[23]

The structure factor of a rigid-rod-type molecule represents a 2D array of rods in the reciprocal space, so-called the Bragg rods (BRs), which extend parallel to q_z through the 2D reciprocal lattice points.[24] The molecular form factor of it depicts a flat oblate ellipsoid with finite thickness ($2\pi/L$, where L is the molecular length). Because GIXD patterns are given by the product of molecular structure factor and form factor, rigid-rod-type molecules contribute to the scattering intensity only at or near a plane orthogonal to the molecular axis. As a result, information of the molecular orientation in preferentially oriented rigid-rod molecules can be obtained from the q_z scattering intensity profile in GIXD patterns. For example, when the rigid-rod-type molecules are uniformly tilted toward the long *b*-axis, then the molecular tilt angle (θ_t) with respect to the surface normal can be calculated by $\tan(\theta_t) = q_z^{(02)}/q_{xy}^{(02)}$.[25]

Experimental Section

Chemical structures of oligofluorene–thiophene derivatives are shown in Scheme 1, and synthetic schemes are well-described elsewhere.[18,19] Hydrophobic surfaces of octadecyltriethoxysilane(OTS)-treated SiO_2/Si substrates were prepared as follows. Precleaned SiO_2/Si substrates were placed in a chamber with a copper block heated to 90 °C and charged with a few drops of pure OTS. The chamber was evacuated to a pressure of about a few millitorr for 5 h. After OTS treatment, the substrates were baked on a hotplate at 110 °C for several minutes, followed by rinsing with isopropyl alcohol to remove excessive OTS molecules. Oligofluorene–thiophene derivatives were then vacuum-deposited on OTS-treated SiO_2/Si substrates with a rate of 0.2–0.3 Å/s under a pressure of $\sim 2.0 \times 10^{-6}$ Torr, in which substrates were kept to 25, 90, and 140 °C, respectively, by a contact heating block during deposition.

(12) Yang, H. C.; Shin, T. J.; Ling, M. M.; Cho, K.; Ryu, C. Y.; Bao, Z. N. *J. Am. Chem. Soc.* **2005**, *127*, 11542–11543.
(13) Qiu, Y.; Hu, Y. C.; Dong, G. F.; Wang, L. D.; Xie, J. F.; Ma, Y. N. *Appl. Phys. Lett.* **2003**, *83*, 1644–1646.
(14) Zhu, Z. T.; Mason, J. T.; Dieckmann, R.; Malliaras, G. G. *Appl. Phys. Lett.* **2002**, *81*, 4643–4645.
(15) Maliakal, A.; Raghavachari, K.; Katz, H.; Chandross, E.; Siegrist, T. *Chem. Mater.* **2004**, *16*, 4980–4986.
(16) Li, D.; Borkent, E. J.; Nortrup, R.; Moon, H.; Katz, H.; Bao, Z. *Appl. Phys. Lett.* **2005**, *86*, 042105.
(17) Vollmer, A.; Jurchescu, O. D.; Arfaoui, I.; Salzmann, I.; Palstra, T. T. M.; Rudolf, P.; Niemax, J.; Pflaum, J.; Rabe, J. P.; Koch, N. *Eur. Phys. J. E* **2005**, *17*, 339–343.
(18) Meng, H.; Bao, Z.; Lovinger, A. J.; Wang, B. C.; Mujsce, A. M. *J. Am. Chem. Soc.* **2001**, *123*, 9214–9215.
(19) Meng, H.; Zheng, J.; Lovinger, A. J.; Wang, B. C.; Van Patten, P. G.; Bao, Z. *Chem. Mater.* **2003**, *15*, 1778–1787.
(20) Locklin, J.; Li, D. W.; Mannsfeld, S. C. B.; Borkent, E. J.; Meng, H.; Advincula, R.; Bao, Z. *Chem. Mater.* **2005**, *17*, 3366–3374.
(21) Especially, x-ray source from the wiggler insertion device is focused through the toroidal mirror and further by K-B mirrors to achieve a higher flux density on the sample, which make it possible to study monolayer (ML) films giving very weak diffraction signals. Furthermore, a CCD area detector was used to supply simultaneous measurements of a wide range of wavevectors in 10 s of exposure time, which is quite advantageous over 1D detectors because it can minimize the radiation damage of radiosensitive organic materials.
(22) The crystal domains composed of randomly oriented crystallites azimuthally on the substrate are described as 2D crystals or 2D powders.
(23) Kuzmenko, I.; Rapaport, H.; Kjaer, K.; Als-Nielsen, J.; Weissbuch, I.; Lahav, M.; Leiserowitz, L. *Chem. Rev.* **2001**, *101*, 1659–1696.
(24) Vineyard, G. H. *Phys. Rev. B* **1982**, *26*, 4146–4159.
(25) (a) Kaganer, V. M.; Möhwald, H.; Dutta, P. *Rev. Mod. Phys.* **1999**, *71*, 779–819. (b) Daillant, J.; Alba, M. *Rep. Prog. Phys.* **2000**, *63*, 1725–1777. (c) Kuzmenko, I.; Rapaport, H.; Kjaer, K.; Als-Nielsen, J.; Weissbuch, I.; Lahav, M.; Leiserowitz, L. *Chem. Rev.* **2001**, *101*, 1659–1696.

Scheme 1. Chemical Structures of Oligofluorene–Thiophene Derivatives with Different End-Substituted Units: (a) Fluorene–Bithiophene–Fluorene (FTTF); (b) 5,5′-bis(7-Hexyl-9*H*-fluoren-2-yl)-2,2′-bithiophene (DHFTTF); (c) 5,5′-bis(7-Dodecyl-9*H*-fluoren-2-yl)-2,2′-bithiophene (DDFTTF)

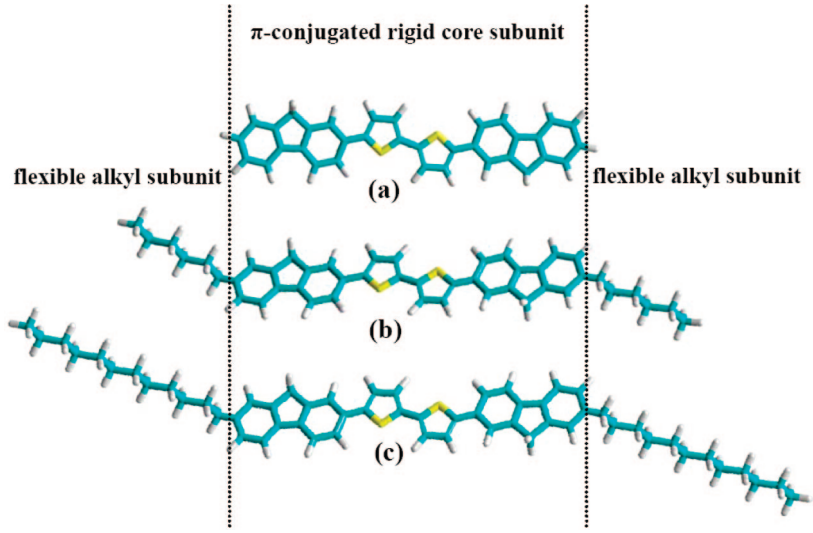

Table 1. Unit-Cell Parameters and Molecular Tilt Angles, As Calculated from the GIXD Patterns of Oligofluorene–Thiophene Derivatives Thin Films, and Field-Effect Mobility in a Top-Contacted Electrode at Various Substrate Deposition Temperatures on OTS-Treated SiO_2/Si Substrates

	T_D (°C)	a (Å)[a]	b (Å)[a]	θ_t (deg)[b]	μ ($cm^2\ V^{-1}\ s^{-1}$)
FTTF	25	5.69	7.92		0.003
	90	5.70	8.10	11.9	0.091
	140	5.78	8.02	12.3	0.073
DHFTTF	25	5.74	8.11	21.6	0.054
	90	5.68	8.61	21.5	0.108
	140	5.80	9.07	26.9	0.117
DDFTTF	25	5.70	8.30	15.5	0.011
	90	5.67	8.21	15.1	0.184
	140	5.70	8.26	16.3	0.143

[a] Rectangular unit-cell parameters. [b] Molecular tilt angle calculated by $\tan\theta_t = q_z^{(02)}/q_{xy}^{(02)}$.

2D GIXD experiments were performed at NSLS X21 beamline at Brookhaven National Laboratory and a monochromator was tuned at 10.5 keV X-rays to minimize radiation damage during measurements. The slightly higher incident angle (~0.3°) than the critical angle of the film (~0.18°) was chosen in order to increase the number of incident photons on the film. The samples were mounted on a translation-tilting stage, and X-ray diffraction patterns were recorded by the MarCCD X-ray detector system. The space between sample and detector was filled with helium gas to remove air scattering. AFM images were acquired by using a Multimode Nanoscope IIIa (Digital Instrument/Veeco Metrology Group).

Results and Discussion

2D GIXD and AFM measurements were carried out for vacuum-deposited 5,5′-bis(9*H*-fluoren-2-yl)-2,2′-bithiophene (FTTF), DHFTTF, and 5,5′-bis(7-dodecyl-9*H*-fluoren-2-yl)-2,2′-bithiophene (DDFTTF) thin films on OTS-treated substrates. Table 1 presents unit-cell parameters, molecular tilt angles (θ_t) in various thicknesses of films and T_D values, and the charge mobility obtained from the corresponding OTFTs.

The OTFTs were fabricated by evaporating the oligofluorene–thiophene derivatives onto OTS-treated SiO_2/Si substrates, consisting of a 300 nm dry thermal oxide dielectric on highly doped silicon, which functions as the gate electrode. The top-contact structures were completed with the deposition of gold source and drain electrodes thru a shadow mask with a $W/L = 10$, where W/L is the ratio of the channel width to the channel length. The field-effect mobility, μ, was calculated using eq 1 from the TFT transfer curves, where I_{DS} is the drain-source current in the saturated regime, C_i the capacitance of the SiO_2 dielectric layer, V_{GS} the gate voltage, and V_T the threshold voltage.

$$I_{DS} = \frac{WC_i\mu}{2L}(V_{GS} - V_T)^2 \quad (1)$$

The characteristic output and transfer TFT curves for 50 nm DHFTTF deposited on OTS-treated SiO_2/Si substrate at $T_D = 90$ °C is shown in Figure 1.

A. Rigid Rod Type FTTF. *A-1. AFM Film Morphology.* Figure 2 presents surface morphologies of FTTF thin films measured at various thickness and T_D values. The grain size of monolayer FTTF islands dramatically increased with elevating T_D. The average grain sizes were about 70 nm, 800 nm, and 1.7 μm at $T_D = 25$, 90, and 140 °C, respectively

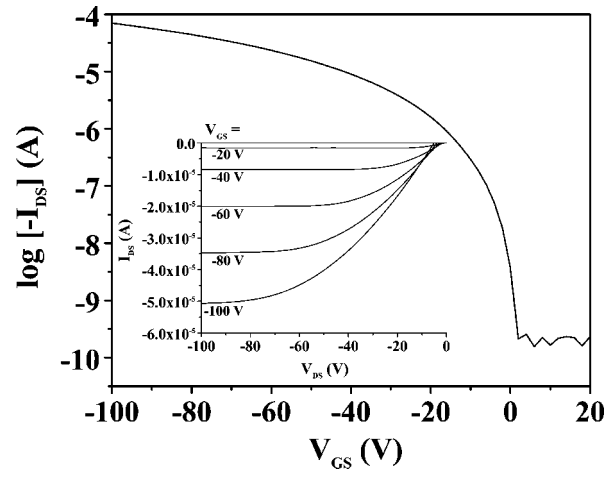

Figure 1. Characteristic output and transfer TFT curves for DHFTTF deposited on OTS-treated SiO_2/Si substrate at $T_D = 90$ °C.

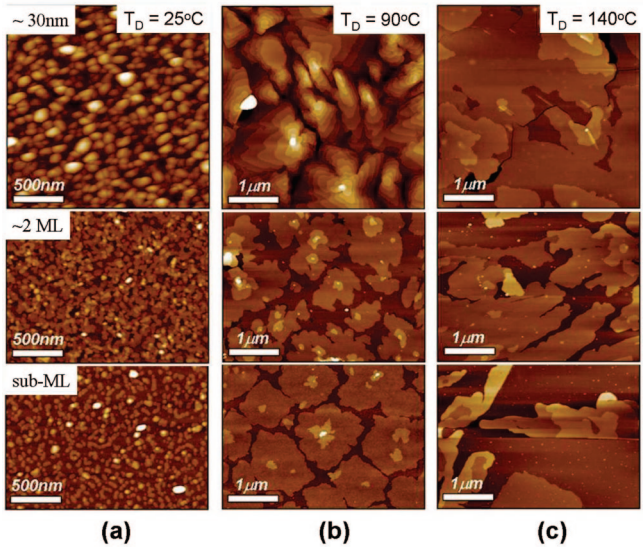

Figure 2. AFM topographs of FTTF thin films deposited on the OTS-treated substrates kept at T_D = (a) 25, (b) 90, and (c) 140 °C.

(see bottom images in Figure 2), which can be understood in terms of the diffusion length. In general, substrate deposition temperature determines the thermal diffusion length, which inevitably influences the grain size. That is, at low substrate temperature, the diffusion length of the FTTF molecules on the substrate surface is very short, resulting in small grains. Thus, the grain size is increased with increasing substrate deposition temperature. At T_D = 25 °C, it shows irregularly layered small crystalline grains, resulting in randomly oriented FTTF crystallites in a 30 nm film. At T_D = 90 °C (see Figure 2b), the monolayer film mostly shows a compact disklike morphology, whereas those of the subsequent layers are close to dendrite. These results suggest that the elevated substrate temperature resulted in a densely packed and well-covered two-dimensional layer. On top of the initial layer, subsequent layers are deposited to make the final terracelike structure shown in a 30 nm film.

The crystalline morphology of films deposited at T_D = 140 °C shown in Figure 2c is quite different from that at other temperatures. Grains are no longer circular but long platelike crystallites. These multilayered crystallites do not display terracelike structures, but stacks of equivalent size of a longish monolayer. Although more experimental evidence and theoretical considerations are necessary to determine the exact growth mechanism, it is nevertheless apparent that very different morphologies are acquired by changing the substrate deposition temperature. The monolayer morphology of T_D = 140 °C suggests that weakly bound admolecules on a hot substrate can overcome an activation barrier (or Ehrlich–Schwoebel barrier[26]) for hopping down a step edge because of their high thermal energy and migrate to sites for further crystal growth. Thus, multilayered crystallites composed of stacks of the equivalent size of longish monolayer can be obtained in a pseudo-layer-by-layer manner.

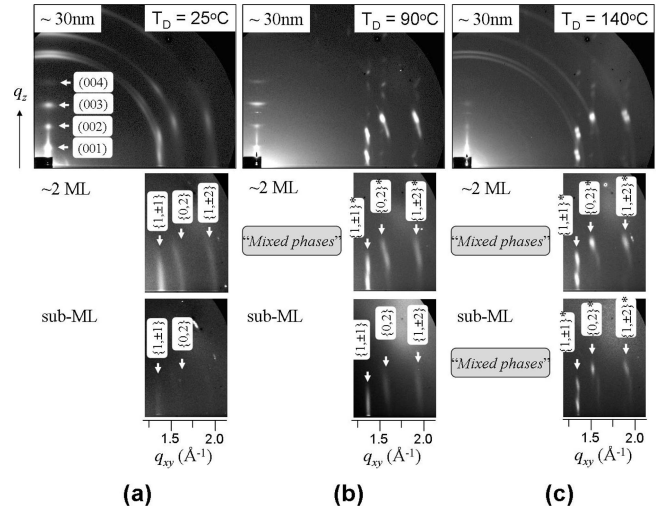

Figure 3. 2D GIXD patterns of FTTF thin films deposited on the OTS-treated SiO_2/Si substrates kept at T_D = (a) 25, (b) 90, and (c) 140 °C.

A-2. 2D GIXD Study. Simple consideration of 2D GIXD patterns from 2D crystals provides useful structural information, that is, three resolved first-order peaks can be indexed to an oblique cell, one nongenerate and one degenerate first-order diffractions to a centered rectangular cell, and only one degenerate first-order peak to a hexagonal cell. Thus, 2D GIXD pattern from the FTTF monolayer shown in Figure 3 can be indexed as a centered rectangular unit cell. The first peak is attributed to the degenerate (*1* ± *1*) reflection and the next one to the nondegenerate (*0 2*) reflection. The third peak is assigned to the degenerate (*1* ± *2*) reflection. It should be noted that the observation of this (*1* ± *2*) reflection strongly suggests that the FTTF crystal consists of a herringbone packing arrangement.[27] Specifically, the peak maxima of (*1* ± *1*) and (*0 2*) reflections appearing at $q_z \neq 0$ Å^{-1} and $2q_z^{(1\pm1)} \approx q_z^{(0\,2)} \approx q_z^{(1\pm2)}$ suggest that the rigid-rod-type molecule has an edge-on orientation to the substrate and is tilted toward its next-nearest neighbors (*NNN* tilt).

The 2D GIXD pattern of sub-ML films of T_D = 25 °C shows weak and broad intensity profiles, suggesting very low crystallinity. Curved Bragg rods (BRs) along the Debye rings, shown in ~2 ML film of T_D = 25 °C (middle of Figure 3a), suggest tilted edge-on structure with quite broad distributions. With increasing film thickness, GIXD patterns become more complicated, indicating irregular stacking of small grains on a cold substrate. GIXD patterns of a 30 nm film show various diffraction peaks, including peaks from the uniformly tilted edge-on structure and ring-shaped diffraction patterns caused by random molecular orientation; split (*1* ± *1*) reflection to the q_z direction resulting from 3D crystals; (*1* ± *1*), (*0 2*), and (*1* ± *2*) reflections parallel to the q_{xy} direction representing face-on structure.

2D GIXD patterns of sub-ML films deposited at T_D = 90 °C (bottom of Figure 3b) represent a typical uniformly tilted, edge-on structure, in which FTTF molecules are tilted toward the *b*-axis by ~12.3° from the surface normal direction. An

(26) (a) Ehrlich, G.; Hudda, F. G. *J. Chem. Phys.* **1966**, *44*, 1039–1049. (b) Schwoebel, R. L.; Shipsey, E. J. *J. Appl. Phys.* **1966**, *37*, 3682–3686.

(27) Durbin, M. K.; Richter, A. G.; Yu, C.-J.; Kmetko, J.; Bai, J. M.; Dutta, P. *Phys. Rev. E* **1998**, *58*, 7686–7690.

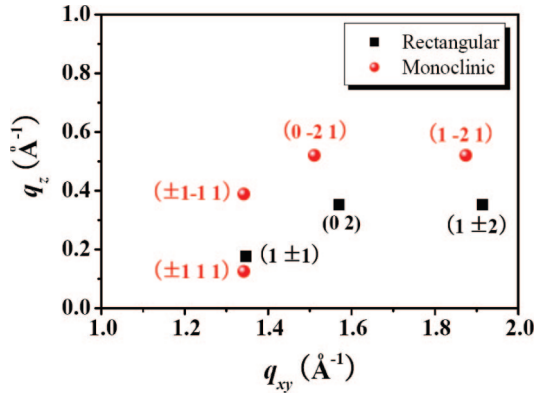

Figure 4. Simulated 2D GIXD patterns for thin film phase with a rectangular unit cell (a_r = 5.74 Å, b_r = 8.01 Å, and θ_r = 12.6°) and multilayer phase with a monoclinic unit cell (a_M = 5.67 Å, b_M = 8.32 Å, c_M = 24.42 Å, α_M = 81.1°, and $\beta_M = \gamma_M$ = 90°).

~2 ML film showed two different crystalline phases, namely the thin film phase and multilayer phase; the thin film phase has a rectangular unit cell with a_r = 5.74 Å, b_r = 8.01 Å, and θ_r =12.6°, whereas the multilayer phase does a monoclinic cell with a_M = 5.67 Å, b_M = 8.32 Å, c_M = 24.03 Å, α_M = 81.1° (θ_M = 8.9°), and $\beta_M = \gamma_M$ = 90°. Interestingly, the tilt angle of the multilayer phase seems slightly smaller than that of the thin film phase, indicating that the interaction of substrate–FTTF molecule is slightly different from that of the FTTF molecules themselves. With above crystal lattice parameters, the positions of maximum intensity in GIXD patterns were simulated and shown in Figure 4. Characteristically, a 30 nm film of T_D = 90 °C (topmost of Figure 3(b)) shows only the thin film phase, suggesting that the long-range-ordered layer-by-layer structure can be acquired by proper tuning of substrate deposition temperature.

The 2D GIXD pattern of a sub-ML film at T_D = 140 °C shows a minority of the thin film phase and a majority of the multilayer phase, which is well consistent with AFM results showing a small portion of a monolayer and mostly multilayered crystallites. A 30 nm film shows diffraction ring patterns indicative of random stacking of grains and GIXD patterns of the thin film phase and the multilayer phase, which again supports the necessity of T_D tuning for the long-range-ordered layer structure.

B. DHFTTF with Flexible Hexyl End-Substituents. Figure 5 represents AFM topographs of ~1 ML, ~2 ML, and 30 nm DHFTTF films vacuum-deposited at various T_D values. The grain size of the interface layer increased from ~100 nm to ~1 μm with increasing T_D. Characteristically, an ~1 ML film of T_D = 25 °C, covering the substrate surface, is well interconnected with small grains. This result is probably related to an enhanced nonpolar–nonpoalr interaction, even on the cold substrate, between hexyl end-substituents of DHFTTF molecules and hairy octadecyl chains of OTS-treated substrate. Highly improved surface coverage achieved by OTS treatment can be understood by considering the surface energy of substrate and DHFTTF thin films. Similar to FTTF, DHFTTF molecules in a vacuum-deposited thin film have edge-on orientation (which will be shown below the GIXD analysis part) on OTS-treated substrate with (*001*) crystal plane corresponding to the surface plane. The surface energy of the plain SiO_2/Si and OTS-treated SiO_2/Si substrates have been reported as 61.4 and 28.1 mJ/m^2, respectively.[28] The reduced surface energy of the OTS monolayer provides a more favorable condition to achieve two-dimensional DHFTTF thin film growth, resulting in a highly improved surface coverage and larger grains. Indeed, the charge-carrier mobility of DHFTTF thin films on OTS-treated substrates showed about two times higher values than that of plain SiO_2/Si substrates (data not shown here). An ~1 ML film deposited at T_D = 90 °C shows dendritic grains, whereas that of 140 °C shows compact disklike grains, demonstrating the tunable crystalline structures with T_D. The subsequent layer of both T_D = 90 and 140 °C, shown in ~2 ML films, displays compact disklike crystalline morphology. Thirty nanometer films of 25 and 90 °C show irregular small grains, whereas that of T_D = 140 °C (Figure 5c) retains the compact disklike morphology throughout the film growth, as confirmed by cross-sectional height profiles of AFM topographs.

Figure 6 represents 2D GIXD patterns of various DHFTTF films with T_D values. Weak and slightly curved (*1 ± 1*) and (*0 2*) reflections (Figure 6a) were observed from an ~1 ML DHFTTF film of T_D = 25 °C, which represent the edge-on structure of small grains and a wide distribution of molecular tilt. The tilt angle to the surface normal, θ_t, calculated from GIXD patterns of ~1 ML films are 21.6, 21.5, and 26.9° for T_D = 25, 90, and 140 °C, respectively. Thirty nanometer films deposited at T_D = 25 and 90 °C showed both edge-on and face-on molecular structure (#-marked peaks) of the thin film phase, whereas the film deposited at T_D = 140 °C shows only edge-on molecular structure. Other structural parameters, including unit-cell dimensions, are listed in Table 1.

C. DDFTTF with Flexible Dodecyl End-Substituents. Figure 7 represents AFM topographs of dodecyl end-substituted DDFTTF thin films. The size of the grains at the dielectric interface, shown in Figure 7a–c, increases with increasing T_D. ~1 ML films of T_D = 25 and 90 °C contain many three-dimensional crystallites, in addition to compact disklike grains. A 30 nm film of T_D = 140 °C (Figure 7d) shows a large amount of crystal nanorods, suggesting that dodecyl end-substituents tend to induce parallel stacks of nanorods on top of the underlying layer.

All 2D GIXD patterns of ~1 ML DDFTTF films in Figure 8 show splitting of diffraction peaks to the q_z direction, suggesting the coexistence of the thin film phase and the multilayer phase, which are consistent with AFM topographs showing a splotchy pattern. The molecular tilt (θ_t), as calculated from 2D GIXD patterns, were 15.5, 15.1, and 16.3° for films deposited at T_D = 25, 90, and 140 °C, respectively. All diffraction patterns of 30 nm films clearly support the mixed structure of edge-on and face-on orientation. As a result, molecular orientation of a 30 nm DDFTTF film can be proposed as shown in Figure 9. The end group edge-on structure shown in Figure 9a was proposed from reflections of circle (1) in Figure 8c; the face-on structure shown in Figure 9b from circle 2 in Figure 8c; and the side

(28) Lim, S. C.; Kim, S. H.; Lee, J. H.; Kim, M. K.; Kim, D. J.; Zyung, T. *Synth. Met.* **2005**, *148*, 75–79.

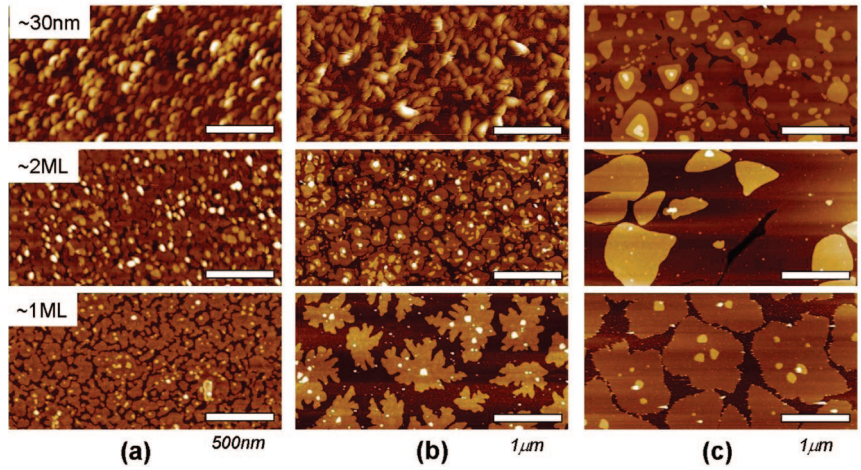

Figure 5. AFM topographs of DHFTTF thin films deposited on the OTS-treated SiO_2/Si substrates kept at T_D = (a) 25, (b) 90, and (c) 140 °C.

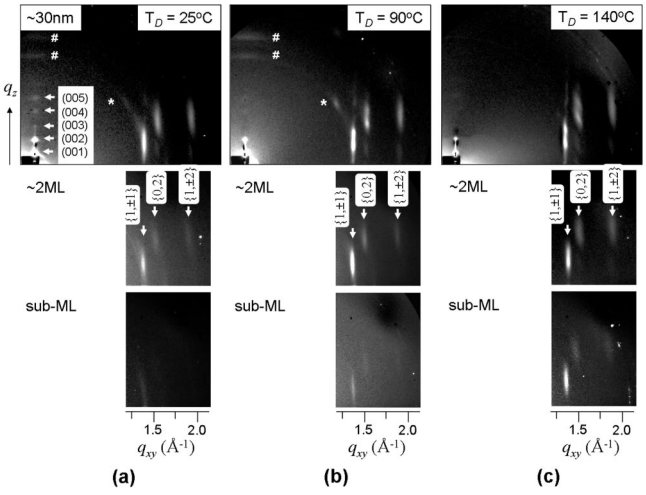

Figure 6. 2D GIXD patterns of DHFTTF thin films deposited on the OTS-treated SiO_2/Si substrates kept at T_D = (a) 25, (b) 90, and (c) 140 °C.

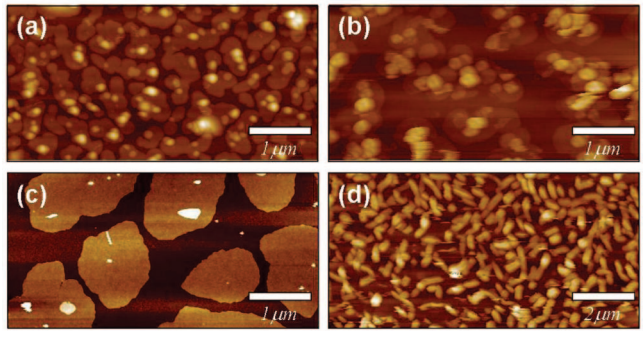

Figure 7. AFM topographs of (a–c) ~1 ML and (d) 30 nm DDFTTF thin films deposited on the OTS-treated substrates kept at T_D = (a) 25, (b) 90, and (c, d) 140 °C.

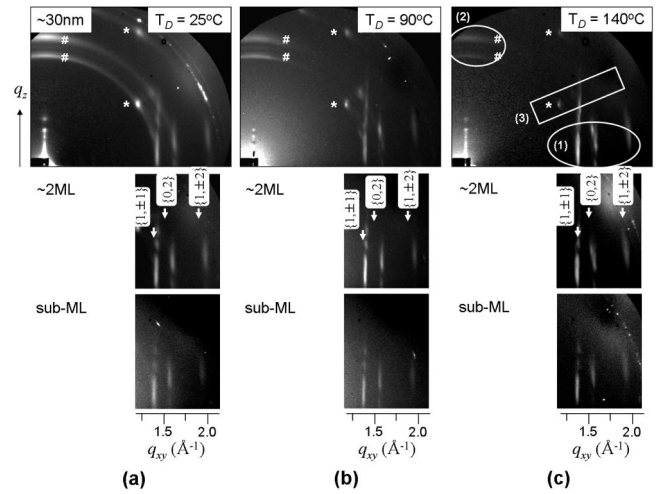

Figure 8. 2D GIXD patterns of DDFTTF thin films deposited on the OTS-treated substrates kept at T_D = (a) 25, (b) 90, and (c) 140 °C.

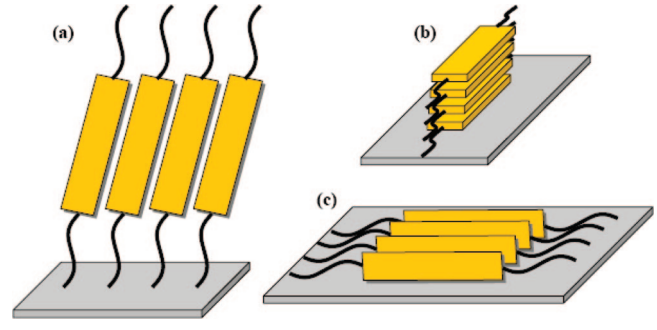

Figure 9. Proposed molecular orientation of DDFTTF molecules based on 30-nm-thck films: (a) end-group edge-on structure; (b) face-on structure; (c) side edge-on structure.

edge-on structure shown in Figure 9c from rectangular (3) in Figure 8c.

D. Effects of Alkyl End-Substituents. The FTTF molecule consists of a fluorene–bithiophene–fluorene π-conjugated core, whereas DHFTTF and DDFTTF molecules include hexyl and dodecyl substituents at the end of the π-conjugated FTTF core, respectively (Scheme 1). Specifically, thin films deposited at T_D = 90 °C were discussed here to investigate overall effects of end substitutions. As previously mentioned, the preferential molecular orientation of FTTF, DHFTTF, and DDFTTF on an OTS-treated silicon oxide surface is the edge-on structure with a surface normal tilt angle of 11.9, 21.5, and 15.1°, respectively. To understand the slightly increased molecular tilt by alkyl end-substitutions, we should consider nonplanarity of a centered π-conjugated core and alkyl subunits. The rigid core is centered between flexible alkyl substituents, which leads to a rigid S-shaped molecule when involved in a close packing. The angle between a conjugated core and the alkyl end-substituent is calculated to ~16° from the energy-minimized molecular

model. While retaining the angle between two subunits, the tilt angle of hexyl and dodecyl substituent to the surface normal direction is calculated at 12 and 9°, respectively, to satisfy the overall tilt angle acquired from GIXD analysis.

The morphology of the thin films, as studied by AFM, is greatly influenced by alkyl end-substituents. The thin film of FTTF at the dielectric interface forms directly, on top of OTS molecules, whereas the subsequent layer is grown onto existing rigid-rod-type of FTTF molecules. The initially seeded grains at the interface will laterally grow until it meets adjacent growing grains or crystal defects caused by structural mismatch with underneath OTS molecules. Interestingly, most nucleation sites for the subsequent layers seem to lie in the center region of the underlying layers (see Figure 2b), and then grow in a radial direction. However, because of structural defects in the edge region of the underlying layer, the growing layer may stop before coalescing. As a result, the overall morphology of a multilayer film represents faceted, terracelike crystallites, similar to a 30 nm FTTF film deposited at a T_D = 90 °C. For alkyl α,ω-substituted DHFTTF and DDFTTF thin films, a similar growth mechanism is observed at the dielectric interface and the subsequent layers, but larger grains are observed because of the stronger intramolecular interactions resulting from the flexible alkyl groups. However, alkyl substituents seem not favorable for the long-range order (i.e., thicker films) of layer-by-layer formation because of their flexibility. A similar trend for DDFTTF has been observed using near-edge X-ray absorption (NEXAFS) technique.[29] Unlike FTTF molecules, alkyl substituted molecules showed mixed structures of both edge-on and face-on molecular orientation, as shown in Figures 5b, 6b, and 8b, at 30 nm films of T_D = 90 °C.

Charge mobility in a top-contacted electrode OTFT device including a DHFTTF semiconducting layer deposited at T_D = 25 °C is 0.054 $cm^2 V^{-1} s^{-1}$, which is quite high considering random stacks of ~100 nm sized small grains and comparing with that of FTTF device deposited at T_D = 25 °C (μ = 0.003 $cm^2 V^{-1} s^{-1}$). This value is only the half-of maximum charge mobility acquired at DHFTTF based device (μ = 0.117 $cm^2 V^{-1} s^{-1}$ at T_D = 140 °C), composed of 10 times larger (~1 μm) grains of the semiconductor layer. These results again support that charge-carrier transport is believed to primarily occur in the first few molecular layers directly in contact with a dielectric layer[5–8] because the well-covered interface layer, composed of uniformly oriented molecules, cause significant improvement of charge mobility. Once the first few layers are formed, the overall morphologies of 30 nm films may not significantly influence the charge mobility because oligofluorene–thiophene derivative based OTFT devices, deposited on a substrate at elevated temperature, showed a modest variation in charge mobility, ranging from 0.073 to 0.184 $cm^2 V^{-1} s^{-1}$. Such variations can be explained by the difference in grain size of the first few nanometers of the film in contact with a dielectric layer.

(29) DeLongchamp, D. M.; Ling, M. M.; Jung, Y.; Fischer, D. A.; Roberts, M. E.; Lin, E. K.; Bao, Z. *J. Am. Chem. Soc.* **2006**, *128*, 16579–16586.

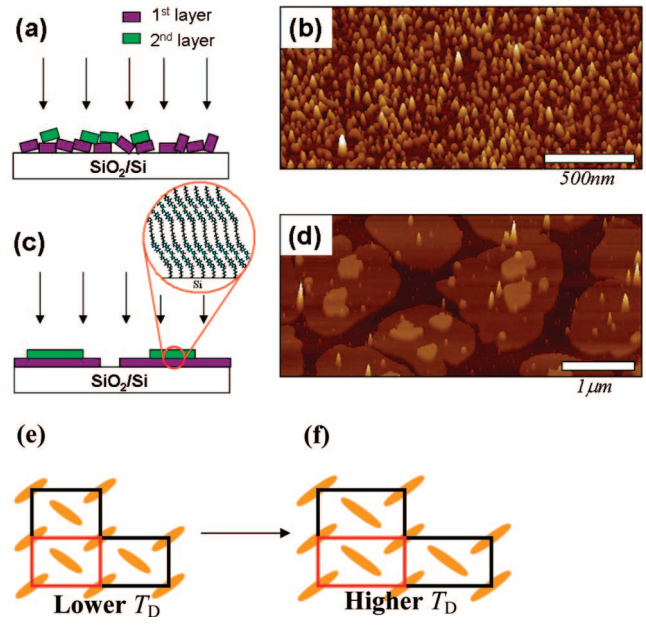

Figure 10. Morphologies of ~ML DHFTTF films: (a) schematic diagram of the ballistic trajectory effects of the first DHFTTF crystals followed by the incident molecules; (b) AFM topography of ~1.5 ML DHFTTF film of T_D = 25 °C; (c) schematic diagram of stacking characteristic of DHFTTF molecules at T_D = 140 °C; (d) AFM topography of a sub-ML DHFTTF film of T_D = 140 °C; (e), (f) schematic drawing for the change of unit-cell dimension with increasing T_D.

E. Effects of Substrate Deposition Temperature (T_D). With increasing substrate deposition temperature, the grain size of the film first few nanometers increased and its grain morphology converted from dendritic to a compact disklike or multilayered structure. Molecular tilts are also increased by a few degrees with increasing T_D. The small increases in tilt angle suggest that as the T_D is increased, molecules within a particular layer are able to achieve a more intimate close-packing through enhanced van der Waals interactions, thus resulting in larger grains. Furthermore, an enhanced crystalline ordering to the out-of-plane direction was also observed with increasing T_D. Peak widths of BRs profiles to q_z direction for the same thickness of samples become narrower, indicative of a longer correlation length to the out-of-plane direction. Furthermore, along the q_z direction, splits of (*1* ± *1*), (*0 2*), and (*1* ± *2*) reflections were observed because of the formation of multilayered structure, which is consistent with increased coherence length at elevated T_D. The sequence of grain sizes at T_D = 90 °C measured from monolayer thickness is FTTF > DHFTTF > DDFTTF, whereas that of field-effect mobility is FTTF < DHFTTF < DDFTTF (see Table 1). These results suggest that even though bigger grains are necessary for high field-effect mobility to decrease grain boundary effect, other factors such as surface coverage, crystal density (or crystal perfection), layer-by-layer interaction, etc., can be important for high charge mobility.

On the basis of GIXD analyses and AFM images, a schematic representation of DHFTTF layers on silicon substrate at T_D = 25 and 140 °C are presented in Figure 10a and c (enlarged AFM topologies are also shown in images b and d in Figure 10). At T_D = 25 °C, grains are quite small and do not align parallel to the substrate, whereas large grains parallel to the substrate are formed at T_D = 140 °C according

to conditions favorable for layer-by-layer growth. Schematic drawings for the change of unit-cell dimension with increasing substrate deposition temperature are also shown in panels e and f in Figure 10, in which the molecular packing arrangement within the unit cell is ascribed to the herringbone motif as the result of 2D GIXD analysis.

Conclusion

Thin-film crystalline structures and morphologies of oligofluorene–thiophene derivatives with different end-substitutions were investigated by 2D GIXD and AFM measurements. It has been found that uniformly tilted edge-on molecular orientation, where π–π stacking planes are parallel to the current flow direction, can be acquired by tuning of molecular structures, substrate treatment such as an OTS monolayer, and substrate deposition temperature. With increasing T_D, the grain size increases with each of the measured oligofluorene–thiophene derivatives. Highly improved two-dimensional growth was achieved by low surface energy of OTS-treated substrate, as observed by AFM, which was correlated with improved charge-carrier mobility. We suggest that the crystallographic and morphological change in the organic semiconductor films caused by changing substrate deposition temperature and surface treatment have a strong impact on its charge carrier mobility in an organic field-effect transistor. 2D GIXD combined with AFM analysis can be widely applied for thin films of various oligomeric derivatives.

Acknowledgment. This work was supported by the United States Department of Energy, Office of Basic Energy Sciences, under Contract DE-AC02-98CH1-886 and the Nanoscale Science and Engineering Initiative of the National Science Foundation under NSF Award DMR-0117792. Z.B. acknowledges partial financial support from the Center for Polymeric Interfaces and Macromolecular Assemblies (NSF-Center MRSEC under Award DMR-0213618). M.R. acknowledges a NASA graduate student research program fellowship.

CM0710599